ACS OMEGA

http://pubs.acs.org/journal/acsodf

Article

Synthesis of Turbostratic Boron Nitride: Effect of Urea Decomposition

Tim Jähnichen,* Jan Hojak, Christian Bläker, Christoph Pasel, Volker Mauer, Valeria Zittel, Reinhard Denecke, Dieter Bathen, and Dirk Enke

Cite This: *ACS Omega* 2022, 7, 33375−33384

Read Online

ACCESS | Metrics & More | Article Recommendations | Supporting Information

ABSTRACT: Since the recent discovery of the template-free synthesis of porous boron nitride, research on the synthesis and application of the material has steadily increased. Nevertheless, the formation mechanism of boron nitride is not yet fully understood. Especially for the complex precursor decomposition of urea-based turbostratic boron nitride (t-BN), a profound understanding is still lacking. Therefore, in this publication, we investigate the influence of different common pre-heating temperatures of 100, 200, 300, and 400 °C on the subsequent properties of t-BN. We show that the structure and porosity of t-BN can be changed by preheating, where a predominantly mesoporous material can be obtained. Within these investigations, the sample BN-300/2 depicts the highest mesopore surface area of 242 m^2 g^{-1} with a low amount of micropores compared to other BNs. By thermal gravimetric analysis, X-ray photoelectron spectroscopy, and Raman spectroscopy, valid details about the formation of intermediates, types of chemical bonds, and the generation of t-BN are delivered. Hence, we conclude that the formation of a mesoporous material arises due to a more complete decomposition of the urea precursor by pre-heating.

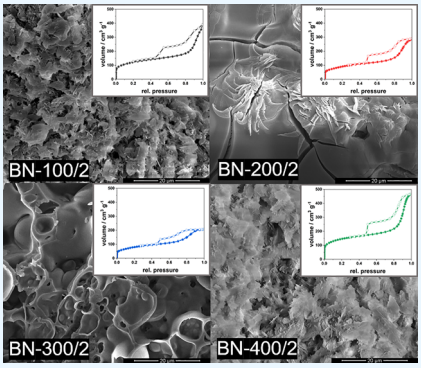

1. INTRODUCTION

During the last few years, there is an increasing interest in advanced porous materials used in catalysis,[1,2] gas storage,[3,4] or water purification.[5,6] One of the materials recently added to that category is hexagonal boron nitride (h-BN).[7−10] Based on its morphology and structure, h-BN can be distinguished into different dimensionalities:[11] 1D boron nitride nanotubes, 2D boron nitride nanosheets, and 3D h-BN. While 1D boron nitride nanotubes and 2D boron nitride nanosheets[12] have been widely studied, extensive investigations are still lacking for 3D h-BN. The 3D form is isostructural to graphite and therefore consists of multiple layers stacked ecliptically on top of each other. These layers are formed by hexagonal rings in which boron and nitrogen atoms are alternating.[13,14] Due to the difference in electronegativity of those two atoms, dipolar interactions take place between the layers, which results in equidistant gaps of around 0.333 nm for h-BN.[15] The particular structure of the material leads to scientifically interesting chemical and physical properties, such as high adsorption affinity for organic substances, high thermal conductivity, and thermal stability up to ∼1000 °C in air.[11,12,16] Compared to other porous materials, however, highly crystalline 3D h-BN has a low specific surface area.[15] Therefore, the synthesis of turbostratic boron nitride (t-BN) is particularly studied. Turbostratic BN emerges by a twisting of the 3D h-BN layers toward one another during the synthesis. Through this structural change, small gaps in the size of micropores arise, which result in increased porosity and decreased crystallinity of the material. Hence, t-BN is characterized by the absence of order in the third dimension and therefore is described as a semi-crystalline material.[17]

Due to the recent progress in the synthesis of porous t-BN, high specific surface areas up to 2078 m^2 g^{-1} can be achieved that makes the material even more attractive for gas and wastewater treatment.[18] However, in past work of Shankar *et al.*,[19] it was depicted that especially defect-rich highly microporous BN exhibits low stability to water, making the material impractical for a variety of applications. Hence, further studies on the BN synthesis are required to enable its practical use in aqueous media. The material can be synthesized using different routes, both template-assisted and template-free. Here, the template-free synthesis is more favored due to its lower number of preparative steps, which leads to a cheaper and more environmentally friendly approach.[20] During template-free synthesis, a solid boron precursor boron oxide or boric acid and a solid nitrogen precursors melamine or urea are often used.[7,20] The precursors are decomposed under a protective gas atmosphere (e.g., nitrogen or ammonia) forming intermediates that later form BN.[20] For the template-free

Received: June 27, 2022
Accepted: August 16, 2022
Published: September 8, 2022

synthesis, the influence of different synthesis parameters such as temperature,[17,21] precursor species,[20,21] and gas-flow rate[9] has been studied so far. Marchesini *et al.*[20] showed the influence of different solid nitrogen sources (urea, melamine, and biuret) on the resulting t-BN. In their study, t-BN with different porosities in dependence of the used nitrogen precursor and its amount was synthesized. It was hypothesized that the porosity of BN can be assigned to the gas release of the solid nitrogen precursors during their decomposition. While, in the case of melamine, an increasing precursor amount showed a higher BET area and porosity, the usage of biuret or urea did not show a linear trend. This observation was explained by the difference in the decomposition mechanism of melamine compared to biuret or urea. Melamine is decomposing in one step (~260 °C), while biuret and urea are decomposing in two steps. In the case of urea, the material starts decomposing at ~150 °C to primary cyanuric acid and biuret.[22] Subsequently, the formed intermediates decompose at higher temperatures to different gases (e.g., CO_2, H_2O, and NH_3).[23]

In this study, the influences of different pre-heating temperatures of 100, 200, 300, and 400 °C and pre-heating times of 2, 4, 6, and 8 h on the synthesis and subsequent properties of t-BN are discussed. While pre-heating steps are commonly known for melamine-based BN,[7,24−26] a profound understanding is still lacking for urea-based BN due to its complex decomposition mechanism (Figure S1). In our work, urea is chosen as the nitrogen precursor due to its disposition to form a BN product with a high amount of mesopores. In previous studies, we were able to conclude that especially mesoporous BN is more water-stable than microporous BN. Hence, we elaborated a simple synthesis approach to modify the porosity of BN to gain a primary mesoporous material by pre-heating. We aim to observe systematic correlations between the chosen pre-heating and the resulting crystallinity, structure, and porosity of t-BN.

In the present synthesis, urea and boric acid are used as starting precursors. Before heat treatment, both precursors are homogeneously mixed in a ball mill. The resulting precursor mixture is heated up via two heating levels to form t-BN. The obtained t-BN was characterized by X-ray diffraction (XRD), X-ray photoelectron spectroscopy (XPS), Raman spectroscopy, scanning electron microscopy (SEM), mercury intrusion, and nitrogen sorption.

2. EXPERIMENTAL SECTION

2.1. Synthesis of BN. To synthesize t-BN, urea (Alfa Aesar, 98+%) and boric acid (VWR Chemicals, 99+%) in a molar ratio of 3:1 were homogeneously ground for 5 min (450 rpm) using a ball mill (PM 100, Retsch, 450). In the physical homogenization no significant changes in crystallinity (Figure S2) and porosity were observed compared to an aqueous homogenization, as already stated in a previous work.[27] The resulting precursor mixture was transferred to an alumina combustion boat crucible (length 20 cm, width 3 cm, depth 2 cm) and heated via two heating levels in a tube furnace (ROC 50/610/14, Thermconcept) under a nitrogen atmosphere (purity of 5.0; flow rate of 150 mL min^{-1}). The first heating level was varied between 100 and 400 °C and maintained between 2 and 8 h. After that, the reaction mixture was heated up further to 1300 °C and maintained for 4 h. During the synthesis, a constant heating rate of 5 K min^{-1} was used. Before removal, the product cooled down to room temperature while maintaining the nitrogen atmosphere. After synthesis, a yield of approximately 80% of a flake-like white BN was obtained. The resulting samples are named BN-T/X, with "BN" referring to boron nitride, "T" to the temperature of the pre-heating level, and "X" to the maintained time of the first heating level in hours.

To investigate BN pre-heating at 300 °C, the prepared precursor mixture was heated with 5 K min^{-1} to 300 °C and maintained for 2 h. After that, the mixture was cooled down to room temperature. During the synthesis, a nitrogen flow of 150 mL min^{-1} was applied.

2.2. Material Characterization. For XRD analysis, a STOE STADIP (STOE & Cie GmbH) with a Mythen 1 K detector (DECTRIS) and CuKα radiation (40 kV, 40 mA) was used. The set step width was 0.2 °2θ s^{-1}. The evaluation of the diffractogram was carried out by Match! (Version 3.3.0, Crystalimpact).

X-ray photoelectron spectroscopy (XPS) used a VG ESCALAB 220i XL measurement device (Thermo Scientific) and an Al-anode (12 kV, 20 mA, 240 W) emitting Al-Kα-radiation. The samples were mounted with a conductive carbon tape. The pressure during measurement was around 10^{-8} mbar, and the measurement range of the electron binding energy was between 5 and 1205 eV with a step size of 0.5 eV at a pass energy of 50 eV. For the detailed spectra, a step size of 0.1 eV was chosen and every scan was repeated four times. For the evaluation of the received spectra, Unifit 2022 was used.[28] Excitation satellites and a suitable background were subtracted. Peaks were fitted by Voigt profiles.

Raman spectroscopy was carried out with a Renishaw inVia Raman spectrometer equipped with a Leica DMI 3000 inverted microscope. To the spectrometer, a CCD camera was attached. As a diode laser source, a Renishaw HPNIR laser (785 nm, 15 W) was used. Additionally, a Cobolt CW DPSS laser (500 mV CW, 45 W) with a 532 or 785 nm laser source was applied.

Morphology was characterized by SEM (Nova NanoLab200, FEI Company) at a voltage of 10−15 kV. The distance of the electron gun to the sample was approximately 5 mm. Before measurement, the samples were sputtered with gold. An Everhart−Thornley detector was used.

Characterization of the pore system of the BN materials followed procedures developed for activated carbons.[29]

Mercury intrusion measurements were used to measure the cumulative pore volume of the macropores. For the measurement, Pascal 140 and Pascal 440 (Porotec) were used. In Pascal 140, the samples were evacuated to 0.2 mbar and then filled with mercury. In Pascal 440, the intrusion measurement up to 400 MPa at room temperature was carried out. The contact angle of mercury was set to 140° and the surface tension to 0.48 N m^{-1}.

Nitrogen adsorption isotherms were measured at 77 K using an autosorb iQ3 (Quantachrome Instruments). Before the measurements, the samples were outgassed under vacuum for at least 4 up to 6 h at 150 °C. To ensure completion of outgassing, the pressure increase had to be less than 25 mTorr min^{-1}. The specific surface areas were determined with the method of Brunauer−Emmet−Teller (BET)[30] according to DIN ISO 9277.[31] The specific mesoporous surface areas (MSA) were determined by using the method of Barrett, Joyner, and Halenda[32,33] according to DIN 66134.[34] The micropore surface areas were determined by using the t-method of Lippens[35] according to DIN 66135,[36] where the

https://doi.org/10.1021/acsomega.2c04003
ACS Omega 2022, 7, 33375−33384

BET area was subtracted from the external surface area. All surface areas were calculated by a mean of at least three reproductions.

The chemical decomposition of urea powder (<63 μm) was investigated by thermogravimetric analysis (TG). As a measuring device, a STA 449 F3 Jupiter (Netsch) was used. For the measurement, approximately 25 mg of the powder was heated in a corundum crucible from room temperature to 500 °C in a nitrogen atmosphere. A heating rate of 5 K min^{-1} was used. In some cases, a specific temperature was held for a certain time before heating to 500 °C.

3. RESULTS AND DISCUSSION

Four different pre-heating temperatures that are close to or within the decomposition range of the precursors were used. Here, 100, 200, 300, and 400 °C were chosen because they are commonly known from previous works of melamine-based BN.[7,24−26] The sample BN-100/2 is pre-heated before any decomposition should occur. The samples BN-200/2 and BN-300/2 are pre-heated within the precursor decomposition of urea and boric acid, and BN-400/2 is pre-heated after the nitrogen precursor is entirely decomposed.

The influence of the pre-heating temperature on the crystallinity of the materials was studied using XRD. As observed in Figure 1, all diffractograms display two broad

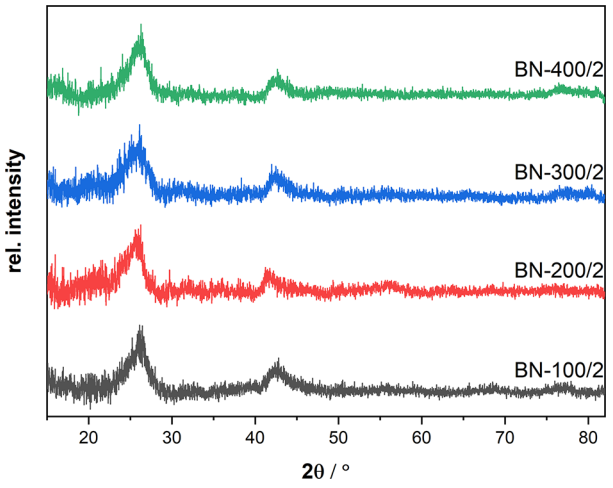

Figure 1. XRD patterns of BN samples synthesized at 1300 °C for 4 h with different pre-heating temperatures from 100 to 400 °C.

reflexes at 2θ = 26 and 43°, and the reflexes can be assigned to the (002) and (10) planes of h-BN.[17,37] Due to the broadness of the reflexes, it cannot be proposed that the material is h-BN. Nevertheless, the synthesis of t-BN is detected. By comparing the reflexes of the samples, only slight changes are observable. Therefore, it can be concluded that the pre-heating temperature has no significant impact on the crystallinity of BN. XPS analysis was used to further investigate the chemical composition and purity of the synthesized t-BN. Figure 2 shows exemplary spectra based on the sample BN-300/2 as no significant differences were observed in dependence on the pre-heating conditions. In Figure 2a, a survey scan spectrum is displayed, revealing only the presence of oxygen, nitrogen, carbon, and boron. The presence of the C 1s and O 1s signals can be attributed to precursor residues from the reaction or adsorbed carbon oxides on the material. The in-depth B 1s and N 1s spectra of BN-300/2 are shown in Figure 2b and Figure 2c, respectively. In the B 1s spectrum, two main contributions at binding energies of ∼193.1 and ∼191.1 eV were obtained. The contribution at the lower binding energy is assigned to B−N and the other one at higher binding energy to B−O. The B−O signal can be explained by the partial decomposition of BN to boron oxide in the presence of water vapor in humid air or by unused boron oxide from the reaction, which is formed during the reaction from dehydrated boric acid. In the N 1s spectrum, the contribution at ∼398.7 eV is attributed to B−N and the contribution at ∼396.8 eV to a B−N defect structure.[38] In both spectra, a shake-up satellite can be observed that may arise by the formation of B−N double bonds within the hexagonal structure of the material.[39] In addition to XPS analysis, Raman spectroscopy was performed. As shown in Figure 2d, the sample depicts a single band at 1375 cm^{-1}, which can be attributed to the E_{2g} mode of h-BN.[40] Other bands could not be observed in the Raman spectrum. By comparing the results received from the XPS and Raman spectra, a successful synthesis of BN with a low amount of impurities (e.g., boron oxide) is proven.

To characterize changes in the morphology of the samples, scanning electron microscopy was used. The samples BN-100/2 (Figure 3a) and BN-400/2 (Figure 3e) exhibit a flake-like morphology as typically displayed by urea-based boron nitride. The samples pre-heated at 200 and 300 °C show a different structure. In both materials, a primarily plain surface can be observed, which is crisscrossed by tubular cracks. As seen in Figure 3b,c, the surfaces are created by stacking of multiple boron nitride flakes that partially show up. Additionally, the sample BN-300/2 shows a second type of morphology (Figure 3d) with many foam-like pores. Similar foam-like pores have been reported by Marchesini *et al.*[27] for urea-rich samples. The change in the morphology compared to the commonly received BN structure (e.g., BN-100/2 and BN-400/2) can be explained by the precursor decomposition and the release of intermediates during the synthesis. To investigate the influence of the urea decomposition on the later structure further, TG measurements in the range of 20−500 °C (5 K min^{-1}) in a nitrogen atmosphere were carried out. In Figure 4a, a complete decomposition of urea is displayed. As already mentioned, urea decomposes in two steps. Figure 4a indicates the first decomposition step in the range of 150−230 °C with a remaining mass of ∼44% at the end of the first step. The lost mass can be attributed to the loss of ammonia and cyanic acid during the formation of, e.g., cyanuric acid, melamine, and biuret from urea (Figure S1).[22] After that, the second decomposition step in the range of 300−375 °C occurs with only ∼6% of the initial mass left. In the second step, it is assumed that, during the decomposition, various gases are produced.[23] Above 375 °C, the leftover residuals start to decompose until ∼450 °C where the material is completely decomposed with less than 1% mass remaining. The impact of an additional pre-heating step during the urea decomposition is shown in Figure 4b,c. In Figure 4b, the temperature was maintained for 2 h at 200 °C, which led to a remaining mass of ∼46% at the end of the heating step. It is expected that, during the reaction, a melt of boron oxide and the decomposed urea residuals is formed above 170 °C. Therefore, by maintaining the temperature at 200 °C, a more homogenized reaction mixture at the given temperature is achieved. Additionally, the formed gaseous decomposition products are released more gently from the reaction melt, resulting in cracks and a more layered structure in the subsequently formed BN (Figure 3b).

https://doi.org/10.1021/acsomega.2c04003
ACS Omega 2022, 7, 33375−33384

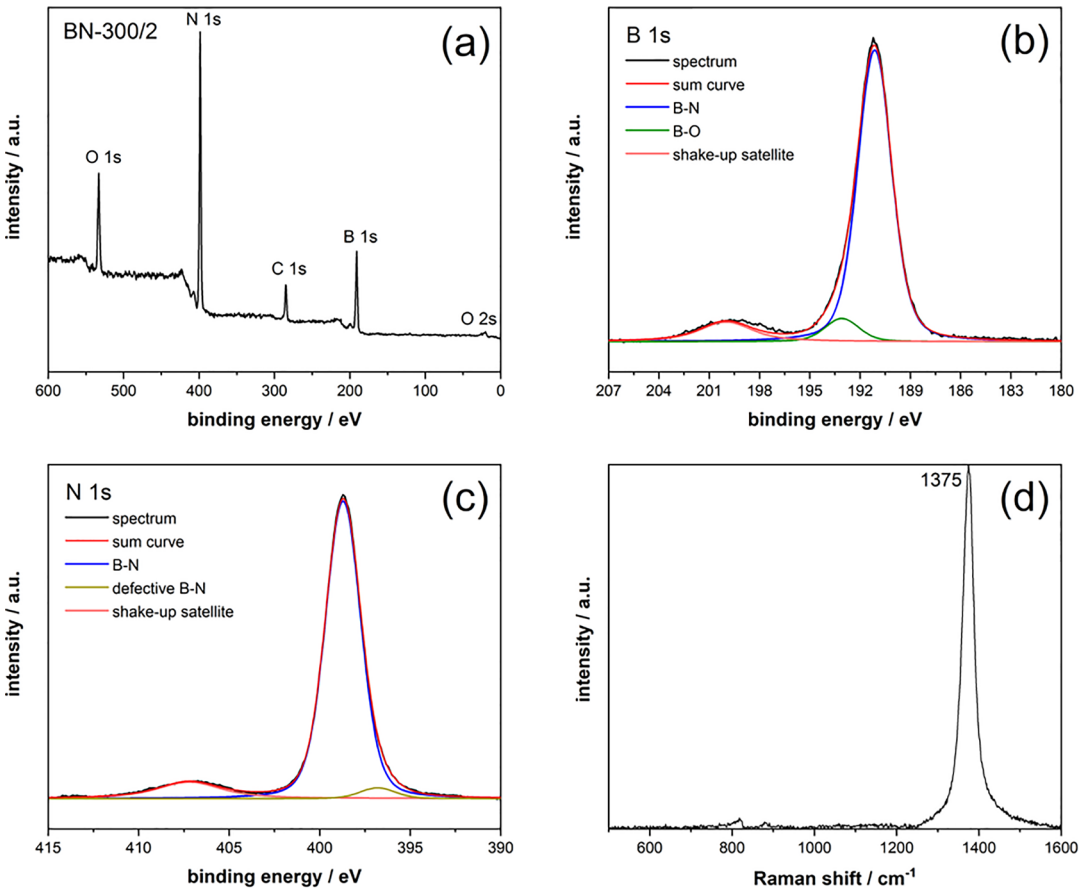

Figure 2. XPS analysis and Raman spectrum of the sample BN-300/2. (a) XPS survey scan spectrum in the range of 0−600 eV. (b) B 1s spectrum. (c) N 1s spectrum. (d) Raman spectrum in the range of 500−1600 cm^{-1}.

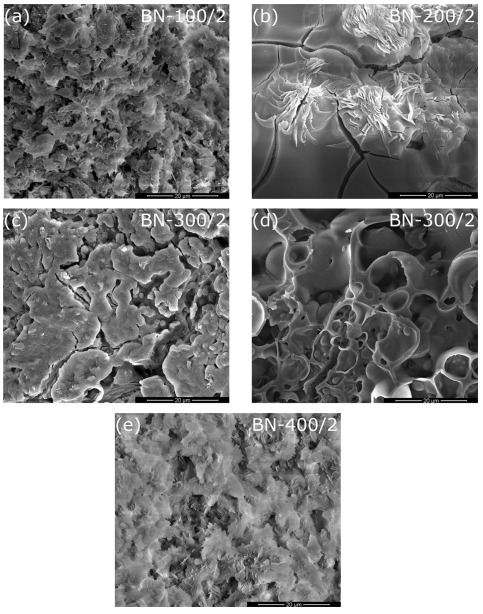

Figure 3. SEM measurements of BN samples pre-heated by (a) 100 °C, (b) 200 °C (c, d) 300 °C, and (e) 400 °C and calcinated at 1300 °C. In the sample BN-300/2, two structures were found. Scale bars are 20 μm.

Therefore, the material synthesized with a pre-heating temperature of 200 °C shows a low amount of macropores. The influence of the pre-heating temperature at 300 °C (2 h) is shown in Figure 4c. As it can be observed, the introduction of a pre-heating step at 300 °C leads to nearly complete decomposition of urea with only ∼9% of the initial mass remaining. As already discussed in the second decomposition step, primarily small gaseous molecules are formed. By releasing these gases from the reaction mixture, the observed vascular foam-like macropores (Figure 3d) are created.

The pore size distribution of the pre-heated samples in the range of 10−10,000 nm was measured by mercury intrusion. As observed in mercury intrusion, the pores in all samples are distributed over a wide range (Figure 5). By comparing the cumulative pore volume, it is noticeable that the samples BN-100/2 and BN-400/2 show a similar pore size distribution with no measurable macropores above ∼3000 nm. In addition, both samples have high cumulative pore volumes with 0.67 $cm^3\ g^{-1}$ (BN-100/2) and 0.73 $cm^3\ g^{-1}$ (BN-400/2). Due to the mercury intrusion results, it can be assumed that the flake-like structure of the samples leads to similar pore size distributions for the macropores and mesopores. Meanwhile, the sample BN-200/2, which has a stacked structure, shows a low cumulative pore volume of 0.36 $cm^3\ g^{-1}$. It is expected that the macropores formed within the material arise due to cracks in the structure as observed by SEM measurements. In general, it can be assumed that a pre-heating at 200 °C leads to a formation of BN with low porosity. For the sample BN-300/2, also, no particular pore size distribution could be measured, but the sample exhibits a higher cumulative pore volume (0.56 $cm^3\ g^{-1}$) than the sample pre-heated at 200 °C. This indicates that, despite a similar stacked structure, the formation

https://doi.org/10.1021/acsomega.2c04003
ACS Omega 2022, 7, 33375−33384

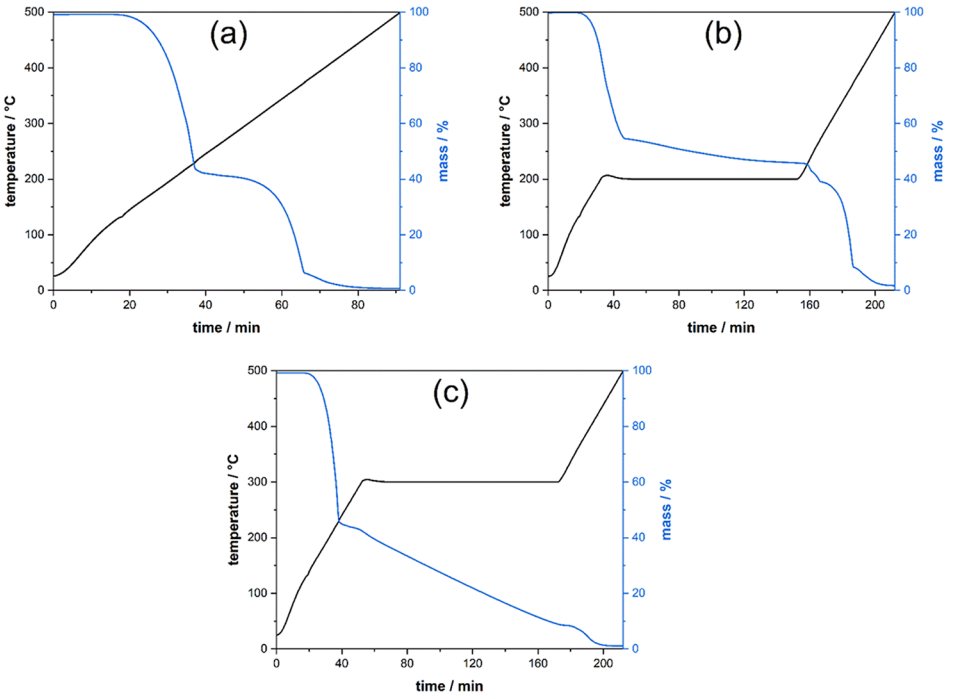

Figure 4. TG measurement of the decomposition of urea in the range of 20−500 °C (a) without any heating step, (b) with a heating step at 200 °C for 2 h, and (c) with a heating step at 300 °C for 2 h.

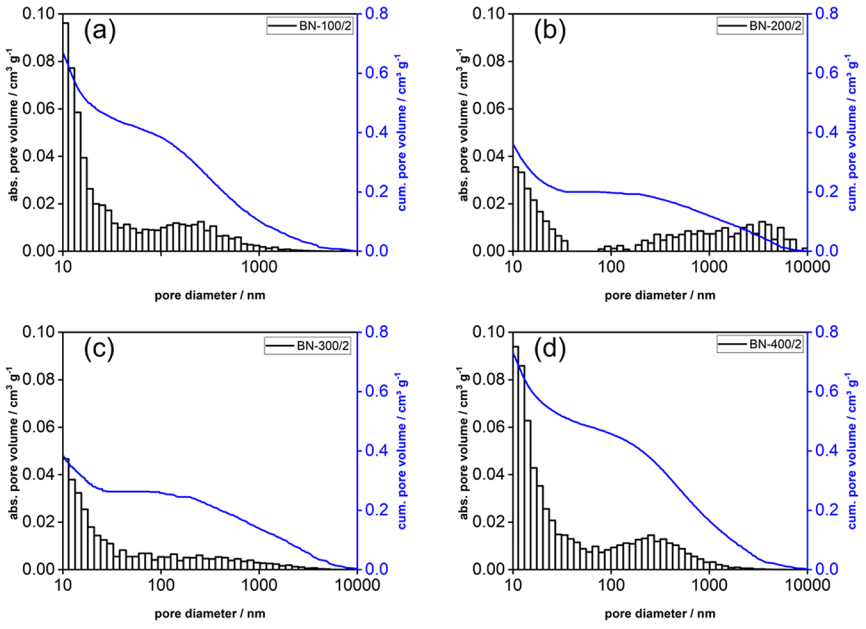

Figure 5. Mercury intrusion measurements of BN samples synthesized at different pre-heating temperatures of (a) 100 °C, (b) 200 °C, (c) 300 °C, and (d) 400 °C.

of the foam pores increases the porosity of the material. To analyze the formation of micropores and smaller mesopores within the material, nitrogen adsorption measurements are used.

The nitrogen sorption isotherms of the four samples pre-heated from 100 to 400 °C are shown in Figure 6. All samples display a similar shape with a steep increase at a low relative pressure followed by a linear to slightly curved ascend, up to a relative pressure of $p\ p_0^{-1} = 0.8$. With a further increase in relative pressure, the steepness of the isotherms increases until a final inflection point is reached at $p\ p_0^{-1} = 1$. The desorption branches show a sharp decrease at a relative pressure of $p\ p_0^{-1} = 0.5$. According to the International Union of Pure and Applied Chemistry (IUPAC) classifications,[41] the isotherms can be classified as type IV(a), which indicates a mesoporous structure. The plateau at high relative pressure is being reduced to an inflection point. The hysteresis loops seem to be a Type H5 hysteresis, which indicates the presence of partially blocked mesopores. The shapes of the isotherms are only slightly influenced by the different heating temperatures. Main differences can be found in the bend after the initial filling of the micropores and at high relative pressure. The samples BN-

https://doi.org/10.1021/acsomega.2c04003
ACS Omega 2022, 7, 33375−33384

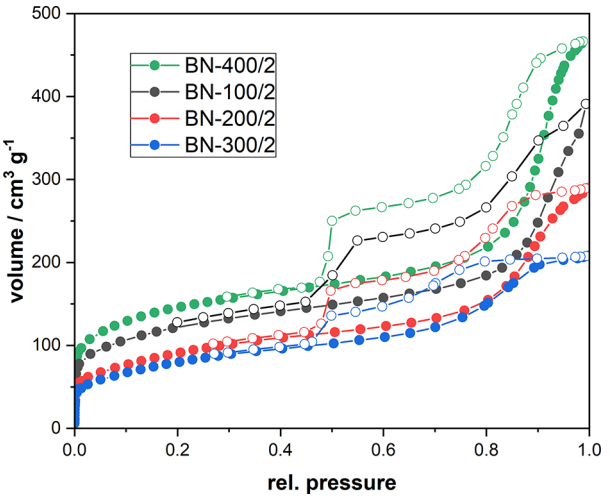

Figure 6. Nitrogen adsorption isotherms of materials with varying pre-heating temperatures between 100 and 400 °C after calcination at 1300 °C.

200/2 and BN-300/2 display a sharper bend, which indicates a complete micropore filling with a very narrow transition region to mesopore adsorption. The other two samples display a less sharp bend. This indicates an overlapping of adsorption in the larger micropores and smaller mesopores for the samples BN-100/2 and BN-400/2. By comparing the adsorption capacities of all samples, a decrease with an increasing pre-heating temperature from 100 to 300 °C can be seen. After that, the adsorption capacity increases again at a pre-heating temperature of 400 °C. In addition, the plateau of the hysteresis loop gets more pronounced up to a pre-heating temperature of 300 °C, indicating partly blocked mesopores. It is supposed that pore blocking occurs due to the formation of a smooth, closed surface, which can be observed in the SEM images. Reichenbach *et al.*[42] concluded that Type IV(a) isotherms with H5-hysteresis loops are attributed to evaporation from blocked and unblocked larger pores at high relative pressures and cavitation inside bottle-shaped pores with narrow bottlenecks, e.g., micropores, at low relative pressures. In Table 1, the mean BET surface areas and the mean mesopore surface areas of the samples are presented. BN-300/2 exhibits the lowest BET area with 281 $m^2\ g^{-1}$ and BN-400/2 the highest with 534 $m^2\ g^{-1}$. Compared to the BET area, the mesopore surface area does not vary as much in between the four samples, ranging from 292 $m^2\ g^{-1}$ for BN-200/2 to 192 $m^2\ g^{-1}$ for BN-400/2. This indicates that most of the changes in the pore volume seem to appear in the range of micropores and smaller mesopores. In comparison to the SEM images presented in Figure 3, similar conclusions can be drawn. Therefore, it can be assumed that, with a pre-heating in the range of 200−300 °C, a template-free synthesis of a purely mesoporous material is possible, which could lead to a higher chemical stability of BN.

As shown by the present results, the pre-heating temperature has a significant impact on the morphology and pore structure of BN. A temperature within the precursor decomposition range (e.g., 200 and 300 °C) leads to extensive changes in its properties, whereas a pre-heating temperature below these decomposition steps (e.g., 100 °C) or above (e.g., 400 °C) has a negligible influence on the material. In the course of this, especially the morphology and pore structure of the resulting BN changes to a denser packed structure with a lower BET surface area. Interestingly, the mesoporous surface area of the materials remained nearly constant. Hence, a pre-heating of urea-based BN at 200−300 °C could lead to solely mesoporous t-BN. Here, the sample BN-300/2 showed, despite a smaller mesopore surface area, a significantly lower micropore surface area and thus a higher amount of mesopores in the material. In addition, the sample did show an interesting foam-like morphology, which is expected to arise by a gas release from the reaction melt during the second urea decomposition step. To further investigate the influence of the pre-heating step at 300 °C, the time of the pre-heated sample has been varied between 2 and 8 h.

The changes in the crystallinity due to the different pre-heating times are examined by XRD. By comparing the received XRD diffractograms in Figure 7, it can be seen that,

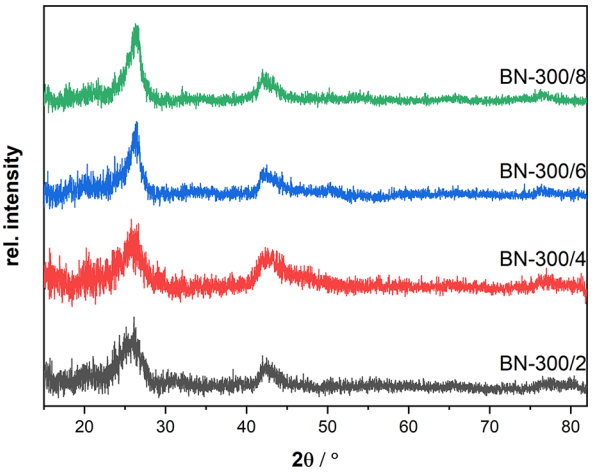

Figure 7. XRD patterns of BN samples synthesized at 1300 °C with different pre-heating times between 2 and 8 h at a pre-heating temperature of 300 °C.

Table 1. Arithmetic Means of the BET, Mesoporous Surface Area, and Microporous Surface Area for All Samples[a]

sample	mean BET surface area ($m^2\ g^{-1}$)	mean mesoporous surface area ($m^2\ g^{-1}$)	mean microporous surface area ($m^2\ g^{-1}$)
BN-100/2	405	224	263
BN-200/2	354	292	194
BN-300/2	281	242	97
BN-400/2	534	192	393
BN-300/4	467	230	274
BN-300/6	399	240	229
BN-300/8	296	216	112

[a]The means are determined from at least three reproductions.

https://doi.org/10.1021/acsomega.2c04003
ACS Omega 2022, 7, 33375−33384

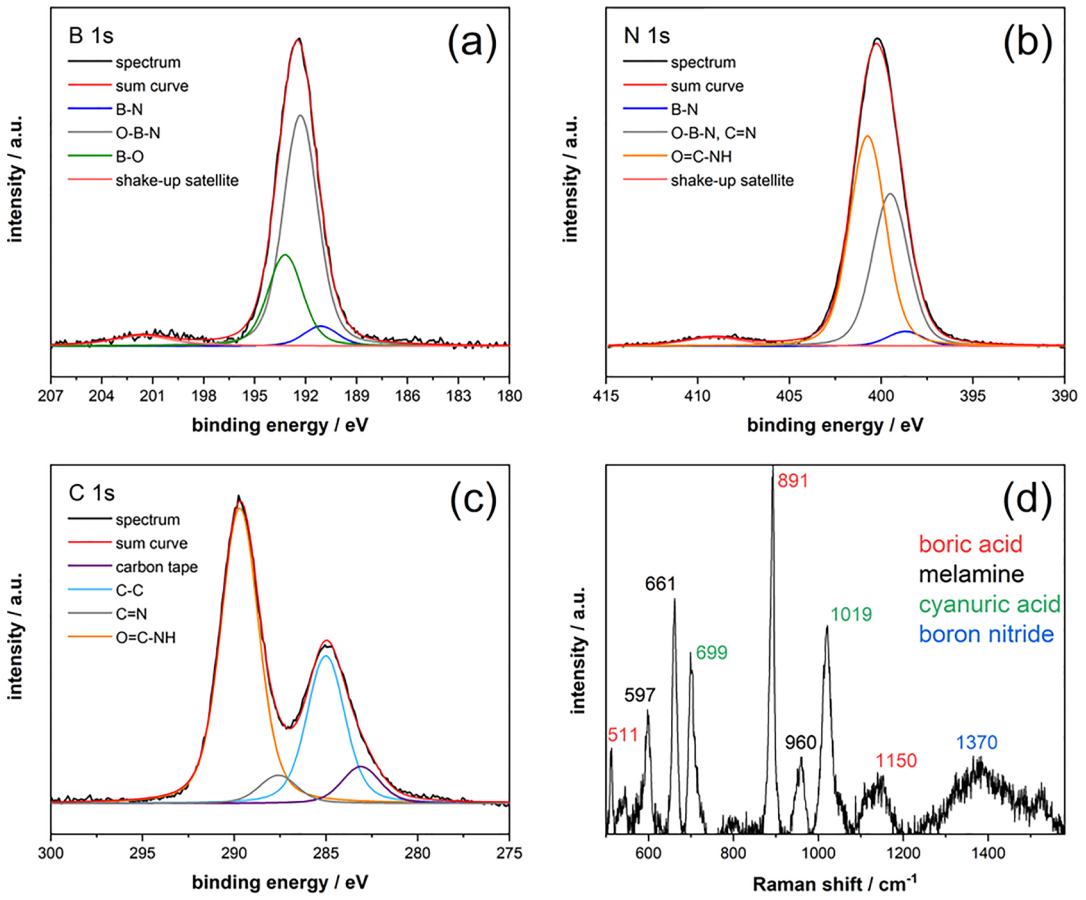

Figure 8. XPS analysis and Raman spectrum of the precursor mixture of boric acid and urea heated at 300 °C for 2 h in a nitrogen flow prior to analysis. (a) B 1s spectrum. (b) N 1s spectrum. (c) C 1s spectrum. (d) Raman spectrum in the range of 500−1600 cm^{-1}.

with increasing pre-heating time, the width of the BN reflexes decreases, and the reflex intensity increases. This suggests that samples synthesized with a longer pre-heating time are more crystalline. Based on the spectroscopic results, two possible reasons for the higher crystallinity due to the longer pre-heating time can be assumed: On the one hand, there may be an increased formation and growth of BN crystallization nuclei at 300 °C,[43] and on the other hand, we propose the reduction of defects in the material by a more complete release of impurities from the reaction mixture. So far, the synthesis of BN at 220−300 °C has been reported by Hubáček *et al.*[44] and Wu *et al.*[43] Hubáček *et al.* synthesized t-BN at 220 °C in vacuum using different boric acid to urea ratios. Wu *et al.* used boric acid, urea, and ammonium tungstate hydrate as precursors. The BN formation was concluded at 300 °C in a nitrogen atmosphere. In both publications, the successful BN formation was identified by XRD. To check if, in the present work, a BN formation starts at 300 °C, XPS and Raman spectroscopy were used because those methods are more suitable to detect t-BN. In Figure 8a and Figure 8b, the received B 1s and N 1s spectra from the XPS analysis are shown, respectively. The B 1s spectrum shows three signals and a shake-up satellite. The contribution at ∼193.1 eV is attributed to a B−O signal, the contribution at ∼192.3 eV to an O−B−N signal, and the contribution at ∼191.1 eV to a B−N signal. In the N 1s spectrum, a shake-up satellite, an O═C−N−H signal at ∼400.7 eV, and a B−N signal at ∼398.7 eV are observed. Additionally, a signal at ∼399.5 eV arises that can be attributed either to O−B−N or C═N.[38] By comparing both spectra, the presence of boron oxide (B−O signal) and a HN═BOH species (O−B−N signal) that are present in the formation of a urea-based BN is detected.[45] It is also assumed that the found shake-up satellite emerges by the double bond present in the HN═BOH species and not by BN due to the intensity of the signals. By comparing the quantification of the B−N signal from the B 1s and N 1s spectra, a ratio of 1:1 is achieved, proving the accuracy of the XPS analysis (Table S1). In Figure 8c, the C 1s spectrum is shown. In the spectrum, a C−C signal at ∼285.0 eV, a C═N signal at ∼287.6 eV, and an O═C−N−H signal at ∼289.7 eV can be found. Also, a signal at ∼281.3 eV resulting from the used carbon tape arises. The signals received in the C 1s spectrum are assigned to the products formed by the urea decomposition. XPS analysis implies the start of the formation of BN due to the presence of the B−N and O−B−N signals. This assumption is supported by the presence of a broad band around 1370 cm^{-1} in the Raman spectrum (Figure 8d), which is presumably BN. The spectrum shows a wide range of bands between 500 and 1600 cm^{-1}. The bands at 511, 891, and 1150 cm^{-1} can be attributed to boric acid.[46] It is assumed that the observed boric acid bands suggest the presence of boron oxide in the reaction mixture due to the rapid reaction of boron oxide to boric acid in air.[47] The remaining bands are affiliated to the decomposition products of urea (i.e., cyanuric acid and melamine presumably).[48,49] Based on the results of the XPS and Raman spectra, the beginning of the BN formation in the range of 300 °C can be confirmed. Therefore, it is assumed that the changes in the crystallinity within the samples BN-

https://doi.org/10.1021/acsomega.2c04003
ACS Omega 2022, 7, 33375−33384

300/2 to BN-300/8 (Figure 7) arise due to an enhanced crystallization of BN with a longer pre-heating time leading to fewer defects within the structure of the material. Hence, by extending the pre-heating time at 300 °C, the crystallinity of the formed BN product is increased.

To observe changes in the morphology of the samples synthesized with different pre-heating times, SEM measurements were used. As shown in SEM images, the foam-like structure that was spotted in the sample BN-300/2 remained in all samples independent from the pre-heating time (Figure S3). Nitrogen adsorption data and the specific surfaces of the samples with varying heating times are presented in Figure 9

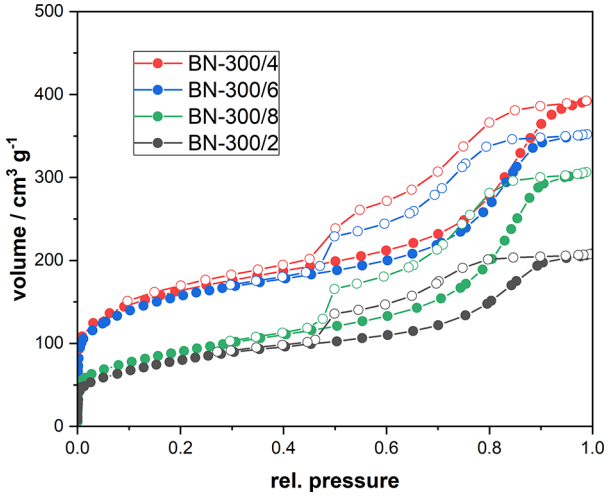

Figure 9. Nitrogen adsorption isotherms after calcination at 1300 °C with 300 °C preheating for 2, 4, 6, and 8 h.

and Table 1, respectively. The general shape of the isotherms is identical to the isotherms discussed above. The BET surface area increases from 2 to 4 h of pre-heating from 281 to 467 m^2 g^{-1}. By extending the pre-heating time, the BET surface area decreases again to 296 m^2 g^{-1} at 8 h. The initial increase in surface area from 2 to 4 h of pre-heating time can be attributed to the incomplete reaction between the precursors in the melt after 2 h, which leads to the formation of additional pores until 4 h. The loss of BET surface area afterward results from the increasing crystallinity of the material and the formation of non-porous h-BN. Despite the changes in the BET area, the mesoporous surface areas of all samples are nearly constant, ranging from 216 m^2 g^{-1} (BN-300/8) to 242 m^2 g^{-1} (BN-300/2). Therefore, the pre-heating time as well as the temperature mainly affects the micropore structure of BN. Again, blocked mesopores of a H5 hysteresis loop might originate from the formation of a smooth surface in the foam-like structures. By the variation of the pre-heating time at 300 °C, the crystallinity and the BET surface area of the resulting products have been modified. Therefore, a longer pre-heating time leads to a more crystalline material. An increase in the crystallinity was assumed by the longer crystallization time of BN and fewer impurities in the reaction melt, which result in fewer structural defects in the subsequent material. In addition, it was shown that, depending on the pre-heating time, different BET areas with similar mesopore surface areas were received. Hence, by changing the pre-heating time at 300 °C, the crystallinity and the BET of BN can be adjusted while almost maintaining the mesopore surface area.

4. CONCLUSIONS

In the present work, we investigated the properties of urea-based t-BN in dependence of different pre-heating steps with various common analytical methods. It was shown that, by varying the pre-heating temperature, the pore structure of BN can be modified. Samples pre-heated at 200 or 300 °C displayed extensive changes in morphology, where a denser structure with a lower cumulative pore volume and BET area was formed. Moreover, those samples showed no reduction in the mesopore surface areas compared to the samples BN-100/2 and BN-400/2. Therefore, the changes in the BET area are primarily driven by changes in the range of micropores and smaller mesopores. Thus, the synthesis with pre-heating in the range of 200−300 °C can be used to produce primarily mesoporous BN, which could be a solution to synthesize a more water-stable material in later studies. By investigating the pre-heating time at 300 °C, we depicted an increase in the crystallinity of BN with a longer pre-heating step. With the aid of XPS and Raman spectroscopy, it was concluded that the higher crystallinity might result from a longer crystallization time of the material or lesser impurities, which lead to lesser defects in the structure.

■ ASSOCIATED CONTENT

Supporting Information

The Supporting Information is available free of charge at https://pubs.acs.org/doi/10.1021/acsomega.2c04003.

X-ray photoelectron spectroscopy quantification, X-ray diffraction analysis of the precursors before and after ball milling, urea decomposition reactions, and scanning electron microscopy images (PDF)

■ AUTHOR INFORMATION

Corresponding Author

Tim Jähnichen − *Institute of Chemical Technology, Leipzig University, Leipzig 04103, Germany;* orcid.org/0000-0002-3795-8453; Email: tim.jaehnichen@uni-leipzig.de

Authors

Jan Hojak − *Chair of Thermal Process Engineering, University of Duisburg-Essen, Duisburg 47057, Germany;* orcid.org/0000-0003-1384-4889

Christian Bläker − *Chair of Thermal Process Engineering, University of Duisburg-Essen, Duisburg 47057, Germany*

Christoph Pasel − *Chair of Thermal Process Engineering, University of Duisburg-Essen, Duisburg 47057, Germany*

Volker Mauer − *Chair of Thermal Process Engineering, University of Duisburg-Essen, Duisburg 47057, Germany*

Valeria Zittel − *Wilhelm-Ostwald Institute for Physical and Theoretical Chemistry, Leipzig University, Leipzig 04103, Germany*

Reinhard Denecke − *Wilhelm-Ostwald Institute for Physical and Theoretical Chemistry, Leipzig University, Leipzig 04103, Germany;* orcid.org/0000-0003-1065-5791

Dieter Bathen − *Chair of Thermal Process Engineering, University of Duisburg-Essen, Duisburg 47057, Germany; IUTA e.V., Institute of Energy and Environmental Technology, Duisburg 47229, Germany*

https://doi.org/10.1021/acsomega.2c04003
ACS Omega 2022, 7, 33375−33384

Dirk Enke − *Institute of Chemical Technology, Leipzig University, Leipzig 04103, Germany;* orcid.org/0000-0001-6610-2948

Complete contact information is available at: https://pubs.acs.org/10.1021/acsomega.2c04003

Author Contributions

T.J. wrote the manuscript, performed the synthesis, measured the mercury intrusion, and interpreted and evaluated the characterization methods. J.H. performed the TG measurements, interpreted the nitrogen sorption, and wrote the evaluation of the sorption measurements in the manuscript under the supervision of C.B. V.M. performed the nitrogen sorption analysis. V.Z. carried out and evaluated the XPS analyses, under the supervision of R.D. C.P., D.B., and D.E. did the conceptualization, funding acquisition, and supervision of the project. All the authors reviewed the manuscript and contributed to the final version.

Notes

The authors declare no competing financial interest.

■ ACKNOWLEDGMENTS

The authors would like to thank L. Saalbach for the preparative support, S. Carstens for the X-ray diffraction measurements, B. Hallack for the scanning electron microscopy analysis, and E. Brade for the Raman spectroscopy measurements. In addition, the Institute of Technical Chemistry at the University of Leipzig and the Chair of Thermal Process Engineering at the University of Duisburg-Essen would like to thank the German Research Foundation (DFG) for financial support within the framework of the DFG projects BA 2012/13-1.

■ REFERENCES

(1) Schüth, F. Poröse Materialien im Überblick. *Chem. Ing. Technol.* **2010**, *82*, 769−777.
(2) Zhang, Y.; Riduan, S. N. Functional porous organic polymers for heterogeneous catalysis. *Chem. Soc. Rev.* **2012**, *41*, 2083−2094.
(3) Morris, R. E.; Wheatley, P. S. Gas storage in nanoporous materials. *Am. Ethnol.* **2008**, *47*, 4966−4981.
(4) Deegan, M. M.; Dworzak, M. R.; Gosselin, A. J.; Korman, K. J.; Bloch, E. D. Gas Storage in Porous Molecular Materials. *Eur. J. Chem.* **2021**, *27*, 4531−4547.
(5) Lv, Y.; Liu, H.; Wang, Z.; Liu, S.; Hao, L.; Sang, Y.; Liu, D.; Wang, J.; Boughton, R. I. Silver nanoparticle-decorated porous ceramic composite for water treatment. *J. Membr. Sci.* **2009**, *331*, 50−56.
(6) Filina, A.; Yousefi, N.; Okshevsky, M.; Tufenkji, N. Antimicrobial Hierarchically Porous Graphene Oxide Sponges for Water Treatment. *ACS Appl. Bio Mater.* **2019**, *2*, 1578−1590.
(7) Li, J.; Lin, J.; Xu, X.; Zhang, X.; Xue, Y.; Mi, J.; Mo, Z.; Fan, Y.; Hu, L.; Yang, X.; Zhang, J.; Meng, F.; Yuan, S.; Tang, C. Porous boron nitride with a high surface area: hydrogen storage and water treatment. *Nanotechnology* **2013**, *24*, 155603.
(8) Ma, R.; Bando, Y.; Zhu, H.; Sato, T.; Xu, C.; Wu, D. Hydrogen uptake in boron nitride nanotubes at room temperature. *J. Am. Chem. Soc.* **2002**, *124*, 7672−7673.
(9) Takagaki, A.; Nakamura, S.; Watanabe, M.; Kim, Y.; Song, J. T.; Jimura, K.; Yamada, K.; Yoshida, M.; Hayashi, S.; Ishihara, T. Enhancement of solid base activity for porous boron nitride catalysts by controlling active structure using post treatment. *Appl. Catal., A* **2020**, *608*, 117843.
(10) Venegas, J. M.; Grant, J. T.; McDermott, W. P.; Burt, S. P.; Micka, J.; Carrero, C. A.; Hermans, I. Selective Oxidation of n -Butane and Isobutane Catalyzed by Boron Nitride. *ChemCatChem* **2017**, *9*, 2118−2127.
(11) Arenal, R.; Lopez-Bezanilla, A. Boron nitride materials: an overview from 0D to 3D (nano)structures. *WIREs Comput. Mol. Sci.* **2015**, *5*, 299−309.
(12) Lin, Y.; Connell, J. W. Advances in 2D boron nitride nanostructures: nanosheets, nanoribbons, nanomeshes, and hybrids with graphene. *Nanoscale* **2012**, *4*, 6908−6939.
(13) Catellani, A.; Posternak, M.; Baldereschi, A.; Freeman, A. J. Bulk and surface electronic structure of hexagonal boron nitride. *Phys. Rev. B* **1987**, *36*, 6105−6111.
(14) Paine, R. T.; Narula, C. K. Synthetic routes to boron nitride. *Chem. Rev.* **1990**, *90*, 73−91.
(15) Kostoglou, N.; Polychronopoulou, K.; Rebholz, C. Thermal and chemical stability of hexagonal boron nitride (h-BN) nanoplatelets. *Vacuum* **2015**, *112*, 42−45.
(16) Zhang, X.; Lian, G.; Zhang, S.; Cui, D.; Wang, Q. Boron nitride nanocarpets: controllable synthesis and their adsorption performance to organic pollutants. *CrystEngComm* **2012**, *14*, 4670.
(17) Alkoy, S.; Toy, C.; Gönül, T.; Tekin, A. Crystallization behavior and characterization of turbostratic boron nitride. *J. Eur. Ceram. Soc.* **1997**, *17*, 1415−1422.
(18) Li, J.; Xiao, X.; Xu, X.; Lin, J.; Huang, Y.; Xue, Y.; Jin, P.; Zou, J.; Tang, C. Activated boron nitride as an effective adsorbent for metal ions and organic pollutants. *Sci. Rep.* **2013**, *3*, 3208.
(19) Shankar, R.; Marchesini, S.; Petit, C. Enhanced Hydrolytic Stability of Porous Boron Nitride via the Control of Crystallinity, Porosity, and Chemical Composition. *J. Phys. Chem. C* **2019**, *123*, 4282−4290.
(20) Marchesini, S.; McGilvery, C. M.; Bailey, J.; Petit, C. Template-Free Synthesis of Highly Porous Boron Nitride: Insights into Pore Network Design and Impact on Gas Sorption. *ACS Nano* **2017**, *11*, 10003−10011.
(21) Weng, Q.; Wang, X.; Bando, Y.; Golberg, D. One-Step Template-Free Synthesis of Highly Porous Boron Nitride Microsponges for Hydrogen Storage. *Adv. Energy Mater.* **2014**, *4*, 1301525.
(22) Schaber, P. M.; Colson, J.; Higgins, S.; Thielen, D.; Anspach, B.; Brauer, J. Thermal decomposition (pyrolysis) of urea in an open reaction vessel. *Thermochim. Acta* **2004**, *424*, 131−142.
(23) Wu, P.; Zhu, W.; Chao, Y.; Zhang, J.; Zhang, P.; Zhu, H.; Li, C.; Chen, Z.; Li, H.; Dai, S. A template-free solvent-mediated synthesis of high surface area boron nitride nanosheets for aerobic oxidative desulfurization. *Chem. Commun.* **2016**, *52*, 144−147.
(24) Örnek, M.; Hwang, C.; Reddy, K. M.; Domnich, V.; Miller, S. L.; Akdoğan, E. K.; Hemker, K. J.; Haber, R. A. Formation of BN from BCNO and the development of ordered BN structure: I. Synthesis of BCNO with various chemistries and degrees of crystallinity and reaction mechanism on BN formation. *Ceram. Int.* **2018**, *44*, 14980−14989.
(25) Örnek, M.; Hwang, C.; Xiang, S.; Xie, K. Y.; Etzold, A.; Yang, B.; Haber, R. A. Effect of synthesis conditions of BCNO on the formation and structural ordering of boron nitride at high temperatures. *J. Solid State Chem.* **2019**, *269*, 212−219.
(26) Xu, X.; Wang, Y.; Wang, Y.; Fu, S.; Wang, C.; Yue, Y.; Wang, Y.; Zhuang, G. Study of one-step pyrolysis porous boron nitride with large specific surface area. *Vacuum* **2020**, *182*, 109769.
(27) Marchesini, S.; Regoutz, A.; Payne, D.; Petit, C. Tunable porous boron nitride: Investigating its formation and its application for gas adsorption. *Microporous Mesoporous Mater.* **2017**, *243*, 154−163.
(28) Hesse, R.. *UNIFIT 2022: Spectrum Processing, Analysis, and Presentation Software for Photoelectron Spectra (XPS), X-ray Absorption Spectra (XAS), Auger Electron Spectra (AES) and RAMAN Spectra.* https://www.unifit-software.de/ (accessed 2021-10-04).
(29) Bläker, C.; Muthmann, J.; Pasel, C.; Bathen, D. Characterization of Activated Carbon Adsorbents − State of the Art and Novel Approaches. *ChemBioEng* **2019**, *6*, 119−138.
(30) Brunauer, S.; Emmett, P. H.; Teller, E. Adsorption of Gases in Multimolecular Layers. *J. Am. Chem. Soc.* **1938**, *60*, 309−319.

(31) *DIN ISO 9277:2014−01, Bestimmung der spezifischen Oberfläche von Festkörpern mittels Gasadsorption - BET-Verfahren (ISO 9277:2010);* Beuth Verlag GmbH: Berlin 2014.
(32) Barrett, E. P.; Joyner, L. G.; Halenda, P. P. The Determination of Pore Volume and Area Distributions in Porous Substances. I. Computations from Nitrogen Isotherms. *J. Am. Chem. Soc.* **1951**, *73*, 373−380.
(33) Joyner, L. G.; Barrett, E. P.; Skold, R. The Determination of Pore Volume and Area Distributions in Porous Substances. II. Comparison between Nitrogen Isotherm and Mercury Porosimeter Methods. *J. Am. Chem. Soc.* **1951**, *73*, 3155−3158.
(34) *DIN 66134:1998−02, Bestimmung der Porengrößenverteilung und der spezifischen Oberfläche mesoporöser Feststoffe durch Stickstoffsorption - Verfahren nach Barrett, Joyner und Halenda (BJH);* Beuth Verlag GmbH: Berlin.
(35) Lippens, B. Studies on pore systems in catalysts V. The t method. *J. Catal.* **1965**, *4*, 319−323.
(36) *DIN 66135−2:2001−06, Partikelmesstechnik - Mikroporenanalyse mittels Gasadsorption - Teil 2: Bestimmung des Mikroporenvolumens und der spezifischen Oberfläche durch Isothermenvergleich;* Beuth Verlag GmbH: Berlin.
(37) Pease, R. S. An X-ray study of boron nitride. *Acta Cryst.* **1952**, *5*, 356−361.
(38) Moulder, J. F., Chastain, J., Eds. *Handbook of X-ray photoelectron spectroscopy: A reference book of standard spectra for identification and interpretation of XPS data, Update*; Perkin-Elmer Corporation, 1992.
(39) Kidambi, P. R.; Blume, R.; Kling, J.; Wagner, J. B.; Baehtz, C.; Weatherup, R. S.; Schloegl, R.; Bayer, B. C.; Hofmann, S. In Situ Observations during Chemical Vapor Deposition of Hexagonal Boron Nitride on Polycrystalline Copper. *Chem. Mater.* **2014**, *26*, 6380−6392.
(40) Geick, R.; Perry, C. H.; Rupprecht, G. Normal Modes in Hexagonal Boron Nitride. *Phys. Rev.* **1966**, *146*, 543−547.
(41) Thommes, M.; Kaneko, K.; Neimark, A. V.; Olivier, J. P.; Rodriguez-Reinoso, F.; Rouquerol, J.; Sing, K. S. W. Physisorption of gases, with special reference to the evaluation of surface area and pore size distribution (IUPAC Technical Report). *Pure Appl. Chem.* **2015**, *87*, 1051−1069.
(42) Reichenbach, C.; Kalies, G.; Enke, D.; Klank, D. Cavitation and pore blocking in nanoporous glasses. *Langmuir* **2011**, *27*, 10699−10704.
(43) Wu, P.; Zhu, W.; Wei, A.; Dai, B.; Chao, Y.; Li, C.; Li, H.; Dai, S. Controllable Fabrication of Tungsten Oxide Nanoparticles Confined in Graphene-Analogous Boron Nitride as an Efficient Desulfurization Catalyst. *Eur. J. Chem.* **2015**, *21*, 15421−15427.
(44) Hubáček, M.; Sato, T.; Ishii, T. A Coexistence of Boron Nitride and Boric Oxide. *J. Solid State Chem.* **1994**, *109*, 384−390.
(45) Men, J.; Li, B.; Li, J.; Li, G.; Chen, J.; Hou, X. Amorphous liquid phase induced synthesis of boron nitride nanospheres for improving sintering property of h-BN/ZrO2 composites. *Ceram. Int.* **2020**, *46*, 8031−8038.
(46) Erdemir, A.; Bindal, C.; Zuiker, C.; Savrun, E. Tribology of naturally occurring boric acid films on boron carbide. *Surf. Coat. Technol.* **1996**, *86-87*, 507−510.
(47) Arenal, R.; Ferrari, A. C.; Reich, S.; Wirtz, L.; Mevellec, J.-Y.; Lefrant, S.; Rubio, A.; Loiseau, A. Raman spectroscopy of single-wall boron nitride nanotubes. *Nano Lett.* **2006**, *6*, 1812−1816.
(48) He, L.; Liu, Y.; Lin, M.; Awika, J.; Ledoux, D. R.; Li, H.; Mustapha, A. A new approach to measure melamine, cyanuric acid, and melamine cyanurate using surface enhanced Raman spectroscopy coupled with gold nanosubstrates. *Sens. & Instrumen. Food Qual.* **2008**, *2*, 66−71.
(49) de Jong, J.; López, P.; Mol, H.; Baeten, V.; Fernández Pierna, J. A.; Vermeulen, P.; Vincent, U.; Boix, A.; von Holst, C.; Tomaniova, M.; Hajslova, J.; Yang, Z.; Han, L.; MacDonald, S.; Haughey, S. A.; Elliott, C. T. Analytical strategies for the early quality and safety assurance in the global feed chain. *Trends Analyt. Chem.* **2016**, *76*, 203−215.

https://doi.org/10.1021/acsomega.2c04003
ACS Omega 2022, 7, 33375−33384